Imaging Features at the Periphery: Hemodynamics, Pathophysiology, and Effect on LI-RADS Categorization

Nikita Consul, MD
Claude B. Sirlin, MD
Victoria Chernyak, MD[1]
David T. Fetzer, MD
William R. Masch, MD
Sandeep S. Arora, MD
Richard K. G. Do, MD
Robert M. Marks, MD
Kathryn J. Fowler, MD
Amir A. Borhani, MD
Khaled M. Elsayes, MD

Liver lesions have different enhancement patterns at dynamic contrast-enhanced imaging. The Liver Imaging Reporting and Data System (LI-RADS) applies the enhancement kinetic of liver observations in its algorithms for imaging-based diagnosis of hepatocellular carcinoma (HCC) in at-risk populations. Therefore, careful analysis of the spatial and temporal features of these enhancement patterns is necessary to increase the accuracy of liver mass characterization. The authors focus on enhancement patterns that are found at or around the margins of liver observations—many of which are recognized and defined by LI-RADS, such as targetoid appearance, rim arterial phase hyperenhancement, peripheral washout, peripheral discontinuous nodular enhancement, enhancing capsule appearance, nonenhancing capsule appearance, corona enhancement, and periobservational arterioportal shunts—as well as peripheral and periobservational enhancement in the setting of posttreatment changes. Many of these are considered major or ancillary features of HCC, ancillary features of malignancy in general, features of non-HCC malignancy, features associated with benign entities, or features related to treatment response. Distinction between these different patterns of enhancement can help with achieving a more specific diagnosis of HCC and better assessment of response to local-regional therapy.

Abbreviations: AP = arterial phase, APHE = AP hyperenhancement, CEUS = contrast-enhanced US, DP = delayed phase, HBP = hepatobiliary phase, HCC = hepatocellular carcinoma, LI-RADS = Liver Imaging Reporting and Data System, LR-M = LI-RADS M, LR-TR = LI-RADS treatment response, PVP = portal venous phase

RadioGraphics 2021; 41:1657–1675

https://doi.org/10.1148/rg.2021210019

Content Codes: CT GI MR OI

From the Department of Radiology, Baylor College of Medicine, One Baylor Plaza, Houston, TX 77030 (N.C.); University of California San Diego Health, San Diego, Calif (C.B.S., K.J.F.); Montefiore Medical Center, Bronx, NY (V.C.); University of Texas Southwestern Medical Center, Dallas, Tex (D.T.F.); University of Michigan Medical School, Ann Arbor, Mich (W.R.M.); Yale School of Medicine, New Haven, Conn (S.S.A.); Memorial Sloan Kettering Cancer Center, New York, NY (R.K.G.D.); Naval Medical Center San Diego, San Diego, Calif (R.M.M.); Northwestern University, Chicago, Ill (A.A.B.); and University of Texas MD Anderson Cancer Center, Houston, Tex (K.M.E.). Presented as an education exhibit at the 2020 RSNA Annual Meeting. Received February 17, 2021; revision requested May 18 and received June 4; accepted June 10. For this journal-based SA-CME activity, the authors C.B.S., V.C., D.T.F., K.J.F., and K.M.E. have provided disclosures (see end of article); all other authors, the editor, and the reviewers have disclosed no relevant relationships. **Address correspondence to** N.C. (e-mail: *nikita.consul@gmail.com*).

[1]Current address: Department of Radiology, Beth Israel Deaconess Medical Center, Boston, Mass.

SA-CME LEARNING OBJECTIVES

After completing this journal-based SA-CME activity, participants will be able to:

- Compare and contrast the techniques used for dynamic contrast-enhanced evaluation of the liver with various imaging modalities.
- Describe the hemodynamics and pathophysiology of various peripheral imaging features that can be seen when evaluating hepatic observations at contrast-enhanced imaging.
- Understand the mimics of hepatic observations with peripheral features and the associated pitfalls of LI-RADS in these scenarios.

See rsna.org/learning-center-rg.

Introduction

Hepatocellular carcinoma (HCC) is currently the fourth most common cause of cancer worldwide and the second leading cause of cancer-related mortality (1). The Liver Imaging Reporting and Data System (LI-RADS) allows noninvasive diagnosis of HCC in at-risk populations without the need for histopathologic confirmation (2). LI-RADS algorithms are based on radiologic features, derived primarily from multiphasic postcontrast imaging (3–7). Careful analysis of the enhancement kinetics of liver observations as well as the distribution and pattern of their enhancement is necessary to increase the accuracy of liver mass characterization. The histologic features,

TEACHING POINTS

- While gadolinium-based and iodinated contrast agents enhance the intravascular space as well as the extravascular interstitial spaces, CEUS contrast agents remain exclusively within the intravascular space.
- Rim APHE is defined as enhancement of the peripheral portions of an observation during the AP due to relative arterialization of the periphery compared with its center.
- Peripheral washout, an imaging phenomenon typically seen only at CT or MRI, is a subtype of washout most pronounced in the periphery of the observation and is suggestive of non-HCC malignancy.
- Rim APHE will peak in the early AP, corona enhancement will peak in the late AP and PVP, while enhancing capsule appearance occurs in the PVP or DP.
- Unlike peripheral washout, nonenhancing capsule appearance is smooth and discrete and shows persistent hypoenhancement in all postcontrast phases.

vascular supply, and vascular drainage of the observations affect their enhancement patterns and the resultant imaging features.

Historically, the presence of arterial phase hyperenhancement (APHE) and washout appearance were considered sufficient for diagnosis of HCC (8), but more recent evidence suggests that the morphology and pattern of enhancement as well as of washout are highly relevant to differentiate HCC from non-HCC malignancies (9), to distinguish recurrent HCC from posttreatment changes, and to potentially differentiate among certain subtypes of HCC (10). As such, LI-RADS version 2018 differentiates between different patterns of enhancement (eg, rim APHE vs nonrim APHE) to maintain high specificity for noninvasive diagnosis of HCC.

This article addresses our current understanding of enhancement patterns along the margins of liver observations and discusses their proposed underlying mechanism for each imaging modality (Table 1). We also review the approach to differentiating these entities. For the purposes of this article, we use the term *peripheral* to refer to imaging features intrinsic to a liver observation that are most pronounced at its periphery, the term *peripheral capsule* to refer to a rimlike structure distinguishable but not separable from the observation, and the term *periobservational* or *perilesional* to refer to imaging features surrounding and extrinsic to a liver observation.

Contrast-enhanced Liver Imaging Techniques

Multiphase contrast-enhanced imaging of the liver can be performed with CT, MRI, and US, provided that minimum acceptable technical parameters are met (29) (Table 2). The imaging modality and pharmacokinetics of the used contrast agent affect the appearance of liver observations (11,30). Regardless of the modality, imaging for HCC requires performance of multiple phases after injection of a contrast agent: late hepatic arterial phase (AP), portal venous phase (PVP), and subsequent phases including the equilibrium phase and delayed phase (DP) (when using extracellular contrast agents), transitional phase and hepatobiliary phase (HBP) (when using hepatobiliary contrast agents), or late phase (when using contrast-enhanced US [CEUS]).

The timing for these contrast-enhanced phases depends on the contrast agent used as well as patient and technical factors (29). Typically for CT and MRI, the late hepatic AP, PVP, and DP or transitional phase are performed with a 30–45-second, 60–75-second, and 3–5-minute delay after injection of contrast material, respectively (31). The HBP, which is specific to the MRI technique when using hepatobiliary agents, is typically performed with a 20-minute delay (32,33).

CEUS relies on agents composed of gas-filled particles encapsulated in a protein or lipid shell (microbubbles or microspheres). Microbubble contrast agents include octafluoropropane gas in a lipid shell, perfluorobutane gas with a phospholipid shell, perflutren in a shell made of human serum albumin, and sulfur hexafluoride gas with a phospholipid shell (34). These particles allow increased US echo generation within the blood pool, which enhances the vascular spaces and microcirculation within and between tissues (11,35). CEUS requires use of a contrast material–specific imaging mode, available as a software upgrade for most modern US systems (29).

While gadolinium-based and iodinated contrast agents enhance the intravascular space as well as the extravascular interstitial spaces (30,36), CEUS contrast agents remain exclusively within the intravascular space. Therefore, the enhancement pattern at CEUS might be different from the patterns seen at CT and MRI for the same underlying observation. Another characteristic of CEUS is that only one observation can be targeted with CEUS at a time, although the rapid contrast material clearance allows multiple injections and interrogation of multiple observations in a single session. APHE may occur rapidly after contrast material injection—often within the first few seconds—and is best detected with continuous viewing, followed by intermittent imaging every 30–60 seconds over a period of 4–6 minutes (or until clearance of contrast material from the liver) to detect the timing and degree of washout, if present (29,34).

Table 1: Main Peripheral and Periobservational Features Described by LI-RADS

Feature	Type	LI-RADS Category	CT or MRI	CEUS
Rim APHE	Peripheral	LR-M	Subtype of APHE mainly in periphery of observation	Subtype of APHE mainly in periphery of lesion
Peripheral washout	Peripheral	LR-M	Subtype of washout mainly in periphery of observation	NA
Targetoid appearance	Peripheral	LR-M	Presence of any of rim APHE, peripheral washout, delayed central enhancement, targetoid diffusion restriction, or targetoid appearance in DP or HBP	NA
Peripheral discontinuous nodular enhancement	Peripheral	Feature of hemangioma	Discontinuous peripheral nodular and globular areas of enhancement in early postcontrast phases with further expansion in subsequent postcontrast phases; the enhancing areas approximately parallel the blood pool	Discontinuous peripheral nodular and globular areas of enhancement in early postcontrast phases that rapidly expand to fill lesion in (or nearly in) its entirety
Enhancing capsule	Peripheral capsule*	Major feature of HCC	Subtype of capsule visible as enhancing rim in PVP, DP, or TP	NA
Nonenhancing capsule	Peripheral capsule*	Ancillary feature of HCC	Subtype of capsule that does not show enhancement in any phase	NA
Corona enhancement	Periobservational	Ancillary feature of HCC	Periobservational enhancement in late AP or early PVP that is contiguous with and surrounds all or part of observation	NA
Arterioportal shunt	Periobservational	NA	Surrounding perfusion defect, appreciated only in late AP, due to compromised venous flow	NA

Source.—References 3–5 and 11–28.
Note.—AP = arterial phase; CEUS = contrast-enhanced US; DP = delayed phase; HBP = hepatobiliary phase; LR-M = probably or definitely malignant, not necessarily HCC; NA = not applicable; PVP = portal venous phase; TP = transitional phase.
*Rimlike structure distinguishable but not separable from the observation.

Overview of Peripheral LI-RADS Features in Different Hemodynamic Phases

An algorithmic approach based on the temporal patterns of peripheral and periobservational enhancement and their morphology can be used to assess for the presence of LI-RADS features (Fig 1).

Visualization of a peripheral rim at noncontrast imaging, across all modalities, is due to central necrotic or cystic changes of the liver observation or to the presence of a capsule. A capsule is commonly hypoattenuating and hypointense at T1- or T2-weighted MRI when compared with the observation or its surrounding liver parenchyma (12,13).

Intravascular contrast material initially arrives at tissues supplied directly by large arterioles. Hyperenhancement during the AP at CT and MRI is due to densely concentrated arteries and arterioles. APHE during the late hepatic AP is due to rapid extravasation of contrast material through leaky capillaries into the interstitium, most commonly in the setting of inflammatory or neoplastic processes. By comparison, only the former mechanism is relevant to CEUS, as the microbubbles are too large to extravasate through even leaky capillaries and mainly contribute to enhancement if intravascular.

APHE at CT or MRI may qualify as an LI-RADS M (LR-M) (probably or definitely malignant, not necessarily HCC) feature, a major feature, ancillary features, or features of benign entities, depending on location and morphology (12,14). On the other hand, APHE at CEUS is due to increased vascular supply or vessel concentration relative to the center, such as in the case of peripheral vessels in a hemangioma or in peripheral vascular tissue with a necrotic, fibrous, or cystic core—for example, in malignancy or abscesses (13,15).

Table 2: Minimum Technical Requirements for LI-RADS Contrast-enhanced Imaging

Imaging Modality	Imaging Unit Parameters	Images Obtained	Contrast Material Parameters
CT	Multidetector CT (≥eight detectors per row)	≤5 mm axial reconstruction, coronal and sagittal MPRs	≥300 mg/mL iodine (1.5–2.5 mL/kg body weight goal dose) injected at 3 mL/sec followed by 30–40 mL saline
MRI	≥1.5-T magnet, torso phased-array coils rather than body coil, and ≥four-channel phased-array surface coils	T2-weighted and DWI sequences at ≤8 mm, contrast-enhanced sequences at ≤5 mm; recommend including T1-weighted and in-phase/out-of-phase gradient-echo sequences	Variable dose dependent on specific agent used; can use ECAs or HBAs
CEUS	Contrast-specific imaging mode Continuous viewing with recording capabilities of 30–60-sec loop	Continuous recording of AP (30–60 sec) Intermittent images every 30–60 sec over period of 4–6 min	Variable dose dependent on specific agent used; followed by 5–10-mL saline flush at 2 mL/sec

Source.—References 11 and 29–41.
Note.—AP = arterial phase, CEUS = contrast-enhanced US, DWI = diffusion-weighted imaging, ECA = extracellular agent, HBA = hepatobiliary agent, MPR = multiplanar reformation.

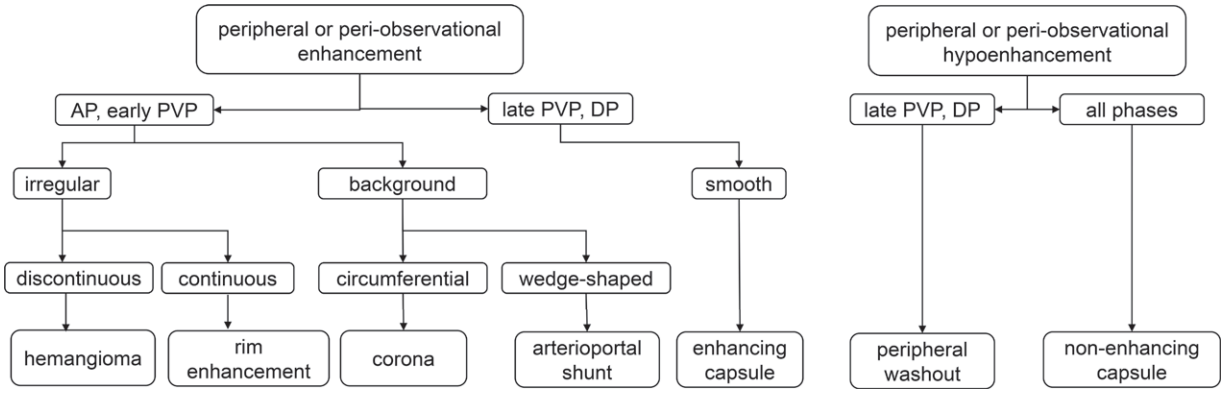

Figure 1. Proposed algorithm for distinguishing between different types of abnormal peripheral or periobservational enhancement.

The PVP is defined by the arrival of contrast material into the portal venous system, which may coincide with the timing of arterially delivered contrast material accumulation in the interstitial tissues. Hypercellular malignant tissues that have a reduced volume of interstitial space will be hypoattenuating or hypointense to the background liver in the PVP and therefore show washout. The exact mechanism of washout at CT and MRI is not fully understood but is thought to be multifactorial, influenced by relative arterial blood flow, relative portal venous blood flow, and the relative volumes of the interstitial and vascular spaces.

Peripheral washout is due to the presence of tissues with high arterial flow, low portal venous flow, and small interstitial volumes at the periphery of a lesion. This pattern could be seen with cholangiocarcinoma, metastases, and some HCCs. Since this pattern is suggestive of cholangiocarcinoma and other non-HCC malignancies, it is considered an LR-M feature by LI-RADS version 2018 (12,14) (further discussed later). At CEUS, washout is purely a function of clearance of the contrast agent from the vascular space and is therefore variable and may be discordant with CT or MRI findings; differential accumulation of contrast material within the interstitial space does not play a role in CEUS (13,15).

In the DP at CT and MRI, contrast material has drained via venous outflow from most tissues but will continue to accumulate in certain areas, such as watery fibrotic tissues with large extracellular spaces. Therefore, enhancement in the DP may be due to the presence of fibrous tissue. When present along the periphery of a lesion, this feature is called an enhancing capsule (since the underlying histologic structure is thought to be either a true tumor capsule or a pseudocapsule), which is recognized by LI-RADS as a major feature of HCC (12,14).

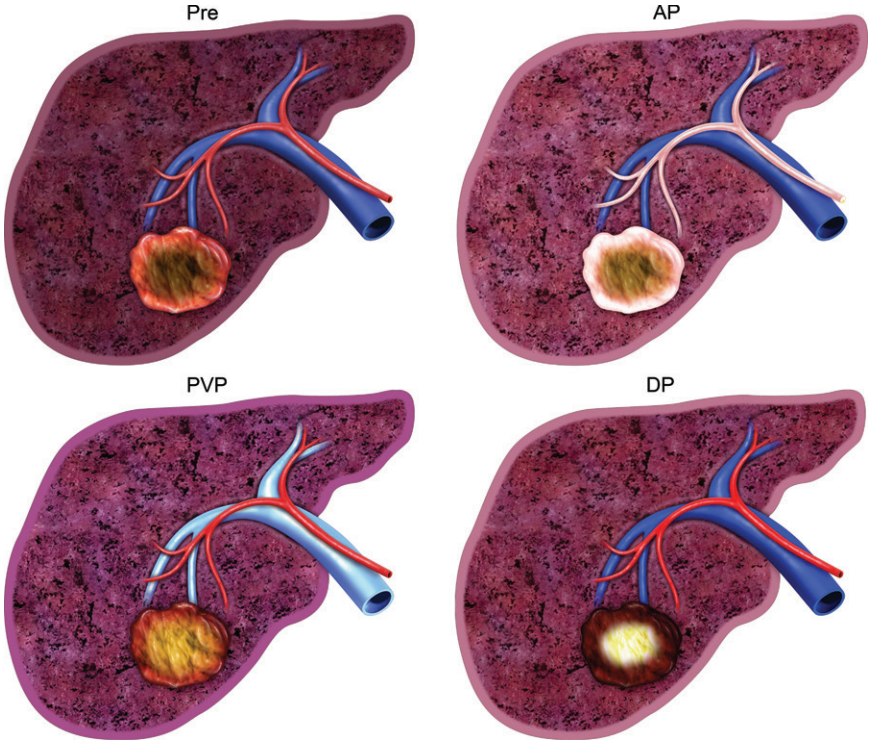

Figure 2. Targetoid appearance includes rim APHE, peripheral washout, central delayed hyperenhancement, DP or HBP targetoid appearance, or any combination thereof. An observation with peripheral washout may be diffusely hypointense on a precontrast *(pre)* image (central connective tissue is dark brown, while peripheral vascularized tissue is pink), but has rim APHE in the AP (peripheral vascularized tissue is now much brighter, while central connective tissue is slightly brighter), which washes out in the PVP (peripheral vascularized tissue is dark orange or pink, while central connective tissue is brighter yellow) and the DP (peripheral tissue is darker than the background liver parenchyma, while central tissue is now much brighter than on the precontrast image); this pattern is concerning for a malignant lesion. Central connective tissue may have delayed hyperenhancement, as in this example, which outlines the peripheral washout.

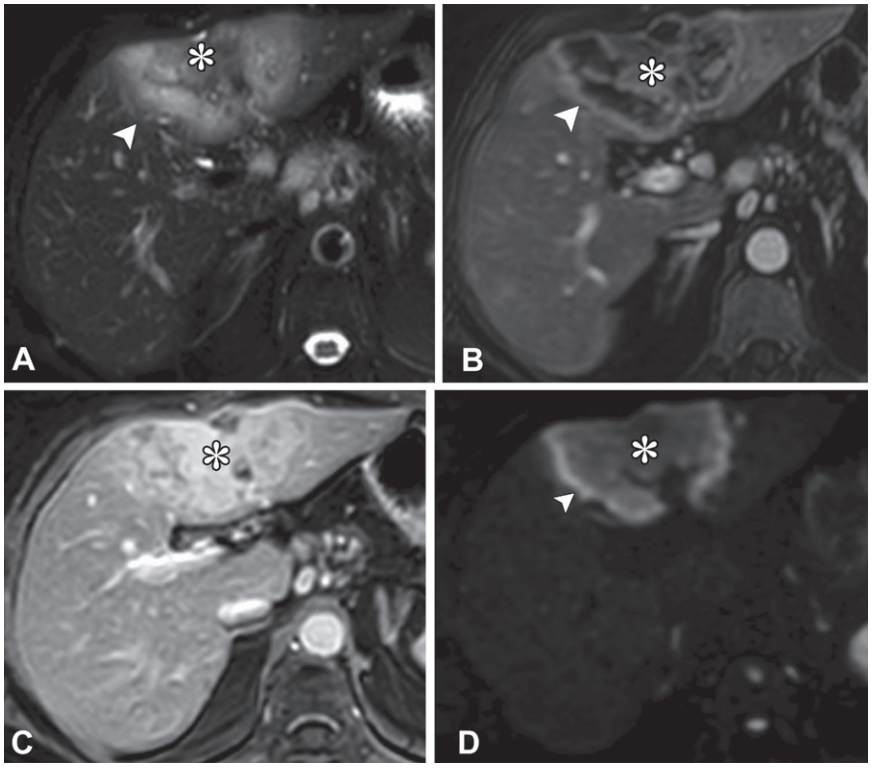

Figure 3. Intrahepatic cholangiocarcinoma (CCA) in a 65-year-old woman with nonalcoholic steatohepatitis (NASH)–related cirrhosis. **(A)** Axial T2-weighted image shows a large mass (*) in the left hepatic lobe with a targetoid appearance (arrowhead). **(B)** On an axial AP MR image, the mass (*) has rim APHE (arrowhead). **(C)** On an axial DP MR image, the mass (*) has progressive central enhancement. **(D)** On an axial diffusion-weighted image, the mass (*) has rimlike hyperintensity (arrowhead).

Peripheral Observational Features

Targetoid Appearance

Targetoid appearance encompasses several imaging features that are suggestive of non-HCC malignancies. These features—which can be seen together or in isolation—include rim APHE, peripheral washout, delayed central enhancement, targetoid diffusion restriction, or targetoid appearance in the DP or HBP (Figs 2, 3) (16). Since these features are nontypical for HCC, they are recognized by LI-RADS version 2018 as LR-M features. Any of these features is sufficient to assign an LR-M category. The differential

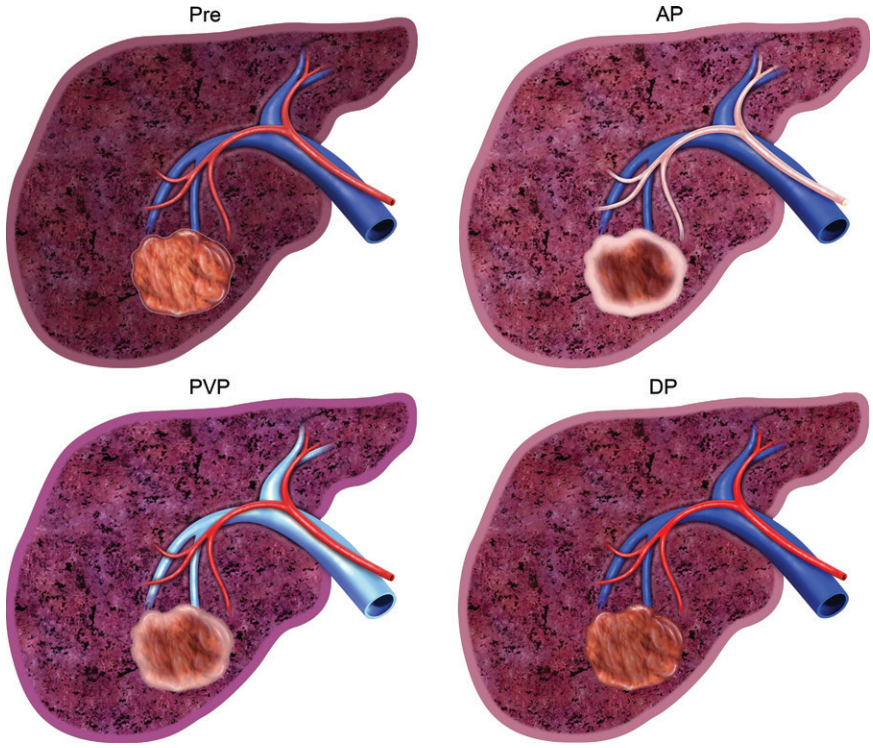

Figure 4. Rim APHE, an LR-M feature with a differential diagnosis that includes metastatic lesion, atypical HCC, or intrahepatic cholangiocarcinoma. It may be isointense to the liver on precontrast *(pre)* images. It manifests as continuous peripheral enhancement in the AP, which fades in the PVP and DP.

diagnosis for lesions with these features includes intrahepatic cholangiocarcinoma, combined HCC-cholangiocarcinoma, atypical HCC, and metastatic lesions (4,17). The underlying pathophysiology of these targetoid features is peripheral hypercellularity and central fibrosis or necrosis.

Rim APHE is defined as enhancement of the peripheral portions of an observation during the AP due to relative arterialization of the periphery compared with its center (Fig 4). It should be distinguished from nonrim APHE, which is a major feature of HCC. The presence of rim APHE is sufficient for LR-M categorization on the basis of CT, MRI, and CEUS LI-RADS version 2018 (Fig 5) (16,18). Rim APHE can be followed by peripheral washout or persist into the DP without washout.

Rim APHE has been shown to be the most sensitive of all LR-M features for non-HCC malignancy, with sensitivity of 71% at MRI (17). Among non-HCC malignancies, it is the most sensitive LR-M feature for combined HCC-cholangiocarcinoma, with sensitivity of 58% and specificity of 85% at MRI (42,43). Benign entities such as infarct (Fig 6), abscess (Fig 7), and sclerosed hemangioma (Fig 8) may also exhibit rim APHE (44–46).

Differentiation of rim APHE from other peripheral enhancement patterns is important. Unlike rim APHE, enhancing capsule (which is a major feature of HCC) is a discrete structure from the lesion seen in the PVP or DP (further discussed later). In addition, the enhancing capsule will not be visible at CEUS (18). Rim APHE can also be confused with corona enhancement (which is an ancillary feature favoring malignancy). In contrast to rim APHE, corona enhancement has ill-defined borders (particularly along its outer edges) and involves the surrounding perilesional tissue. Rim APHE may be irregular and incomplete, mimicking a hemangioma. However, a hemangioma will have nodular and discontinuous peripheral enhancement during the AP.

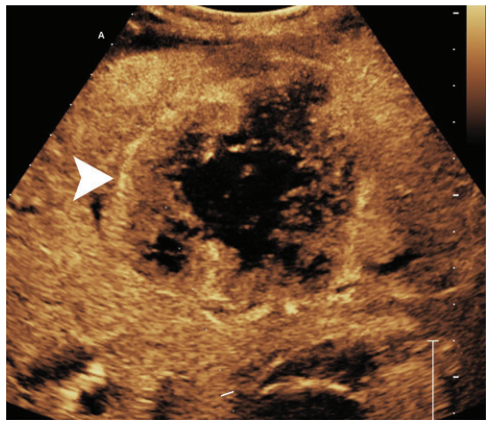

Figure 5. Rim APHE in a 60-year-old woman with chronic liver disease and lung cancer. Image from late AP CEUS shows a heterogeneous lesion with rim APHE (arrowhead) and a central area of nonenhancement (due to necrosis). CEUS LI-RADS category LR-M was assigned. Percutaneous biopsy demonstrated metastatic lung cancer.

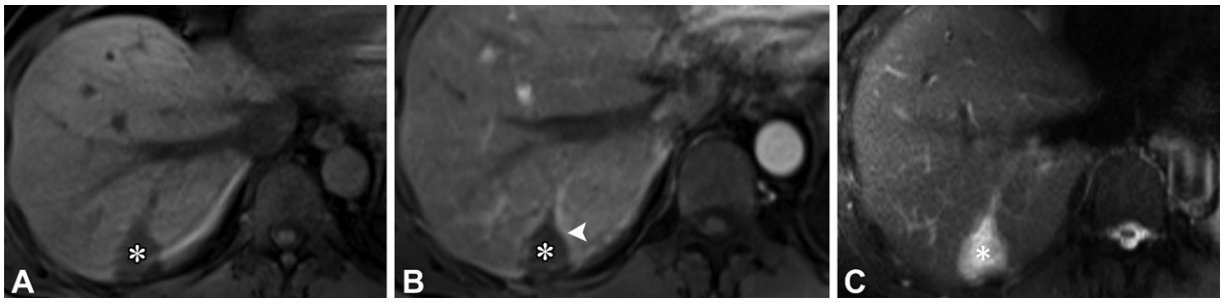

Figure 6. Hepatic infarct in a 46-year-old woman with a pulmonary embolism. **(A)** Axial noncontrast T1-weighted image shows a hypointense wedge-shaped observation (*) in segment VII. **(B)** On an axial postcontrast AP T1-weighted image, the observation (*) has rim APHE (arrowhead). **(C)** Axial T2-weighted image shows hyperintense signal within the observation (*). The findings are most compatible with a perfusion defect due to hepatic infarct in the setting of an ongoing thromboembolic process.

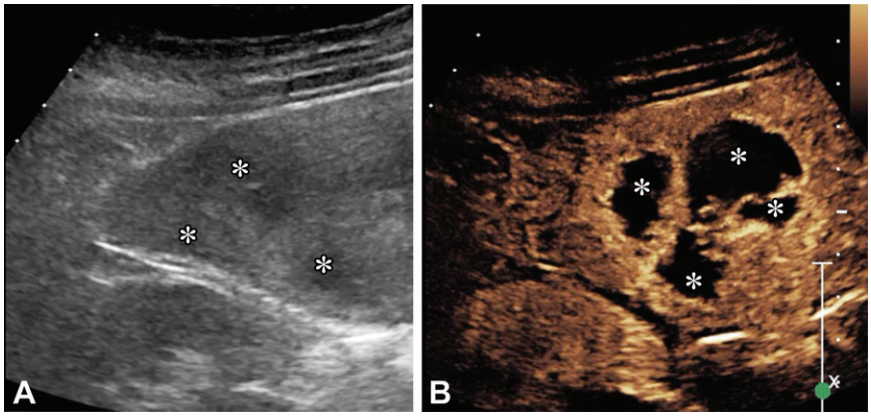

Figure 7. Pyogenic hepatic abscess in a 54-year-old woman with sepsis and gram-positive bacteremia. **(A)** Gray-scale US image through the inferior tip of the right lobe shows an ill-defined multilobulated hypoechoic area (*). **(B)** Image from late AP CEUS shows a multiloculated mass with well-defined rim APHE. Abscess was suspected on the basis of absence of enhancement in the central aspect of the lesion (*) and the patient's clinical condition. The percutaneous aspirate grew *Klebsiella pneumoniae*.

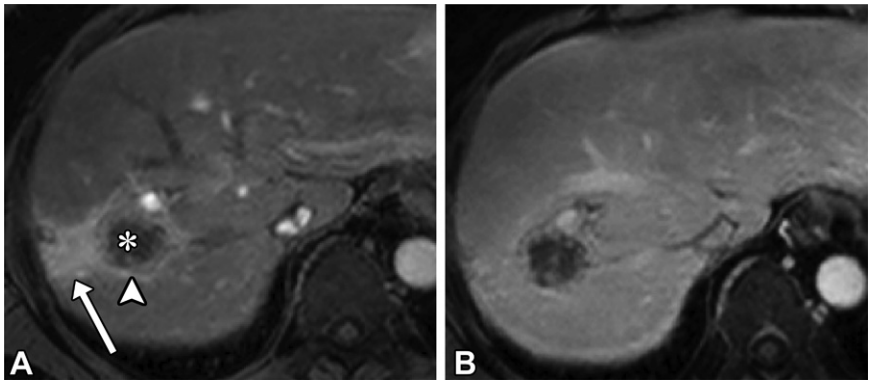

Figure 8. Sclerosed hemangioma in a 61-year-old man. **(A)** Axial AP MR image shows a mass (*) with rim APHE (arrowhead). **(B)** Axial PVP MR image shows that the rim APHE persists in the PVP. The mass did not have fluorodeoxyglucose (FDG) uptake at PET (not shown). The lesion was biopsied and was pathologically proved to be a sclerosed hemangioma. Note the arterioportal shunt (arrow in **A**) just peripheral to the lesion, which is better seen in the AP and fades in the PVP.

Peripheral washout, an imaging phenomenon typically seen only at CT or MRI, is a subtype of washout most pronounced at the periphery of the observation and is suggestive of non-HCC malignancy. Peripheral washout is usually not seen or seen only faintly with CEUS, and it is not used in CEUS LI-RADS (18). The underlying pathophysiology is hypercellularity of the peripheral part of the lesion with relatively small interstitial volume, resulting in diminished accumulation of contrast material during the PVP and DP (19).

Peripheral washout can be seen in mass-forming intrahepatic cholangiocarcinoma (Figs 9, 10). In contrast, abundant loose connective tissue in the central part of cholangiocarcinoma contains a high amount of extracellular volume, which results in delayed retention of extracellular contrast material at CT and MRI, further accentuating the peripheral washout. Atypical and scirrhous HCC has also been shown to have peripheral washout in some cases, although this is not classic (47).

Targetoid diffusion restriction is defined as concentric diffusion restriction at the periphery of an observation (Fig 3). Targetoid HBP appearance is another targetoid feature, referring to relative hyperintensity in the central portion of an observation during the HBP (16). This appearance is due to retention of contrast material in the central fibrotic portion of a lesion with moderate abundant extracellular space (20).

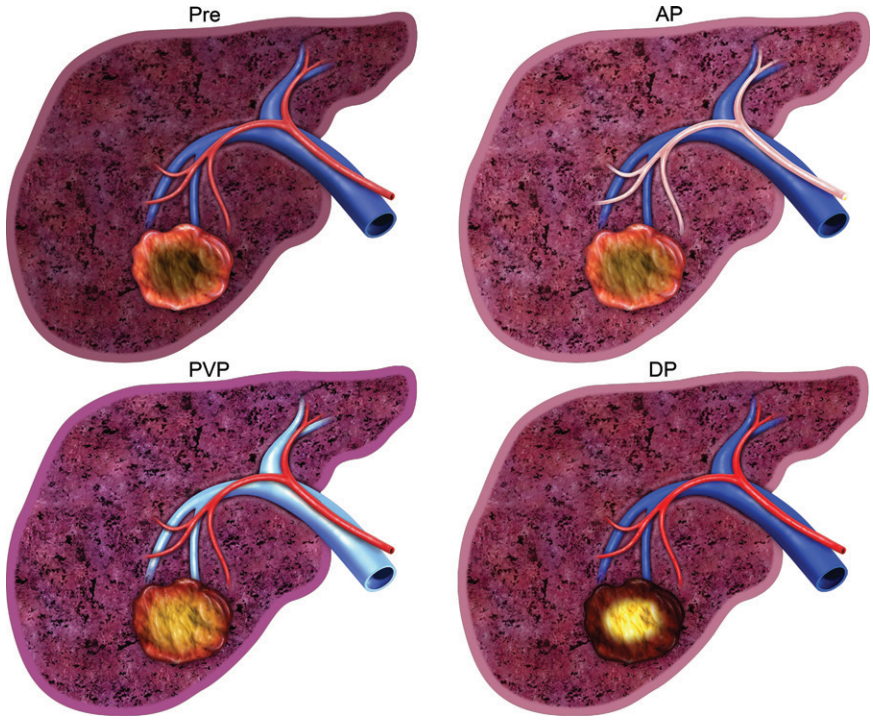

Figure 9. Peripheral washout is an LR-M feature highly suggestive of malignancy but not specific for HCC. An observation with peripheral washout may be diffusely hypointense on precontrast *(pre)* images (orange-pink peripheral vascularized tissue surrounds a central fibrous dark yellow tissue core), but has peripherally vascularized tissue that washes out in the PVP and DP (peripheral orange-pink tissue becomes progressively darker in the PVP and DP). Central connective tissue may be nonenhancing or hyperenhancing, which makes the peripheral washout more prominent (in this example, the central fibrous core is slightly brighter in the DP with enhancement).

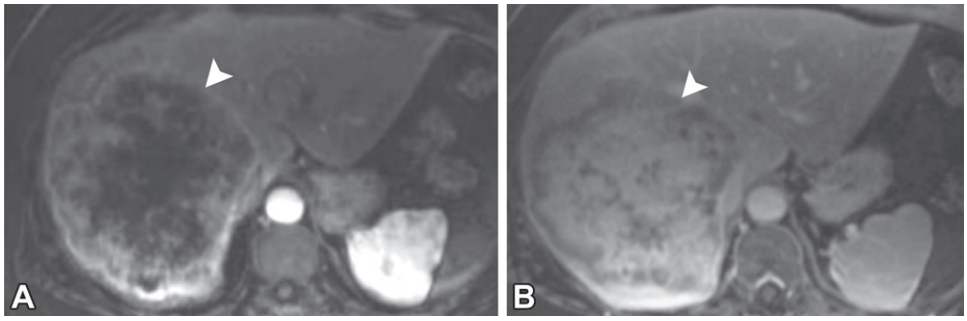

Figure 10. Intrahepatic cholangiocarcinoma in a 53-year-old man with right upper quadrant pain and weight loss. **(A)** Axial postcontrast AP T1-weighted image shows a mass with rim APHE (arrowhead). **(B)** Corresponding image in the PVP shows peripheral washout (arrowhead), with concomitant central intralesional enhancement.

Peripheral Discontinuous Nodular Enhancement

Peripheral discontinuous nodular enhancement is the enhancement pattern characteristic of hemangioma. The nodular component of enhancement progressively increases in size centripetally and parallels the blood pool (Figs 11, 12) (21). This type of enhancement pattern should not be confused with continuous peripheral irregular enhancement, which is a form of rim APHE and can be seen in non-HCC malignancies. Changes after local-regional treatment may also result in peripheral nodular enhancement (Fig 13). It should also be distinguished from satellite nodules surrounding an intrahepatic malignancy, which are a feature of intrahepatic metastasis associated with microvascular invasion (48–50).

Hemangiomas in cirrhotic liver may not exhibit the typical peripheral discontinuous nodular enhancement pattern. Hemangiomas in these patients may show rapid homogeneous enhancement or continuous peripheral nodular enhancement (21,51). Attention to other imaging findings (such as signal intensity characteristics on T2-weighted images) and comparison with prior imaging studies are helpful to differentiate atypical hemangiomas from malignant lesions. Over time, the hemangioma may undergo involution and sclerosis of vascular spaces and subsequently exhibit rim APHE (Fig 8) (51).

Peripheral Capsule

Enhancing Capsule Appearance

A fibrous capsule (FC) is specific to HCC and is rarely encountered with other tumors (52). FCs associated with HCC are composed almost entirely of collagen fibers and are thought to be per-

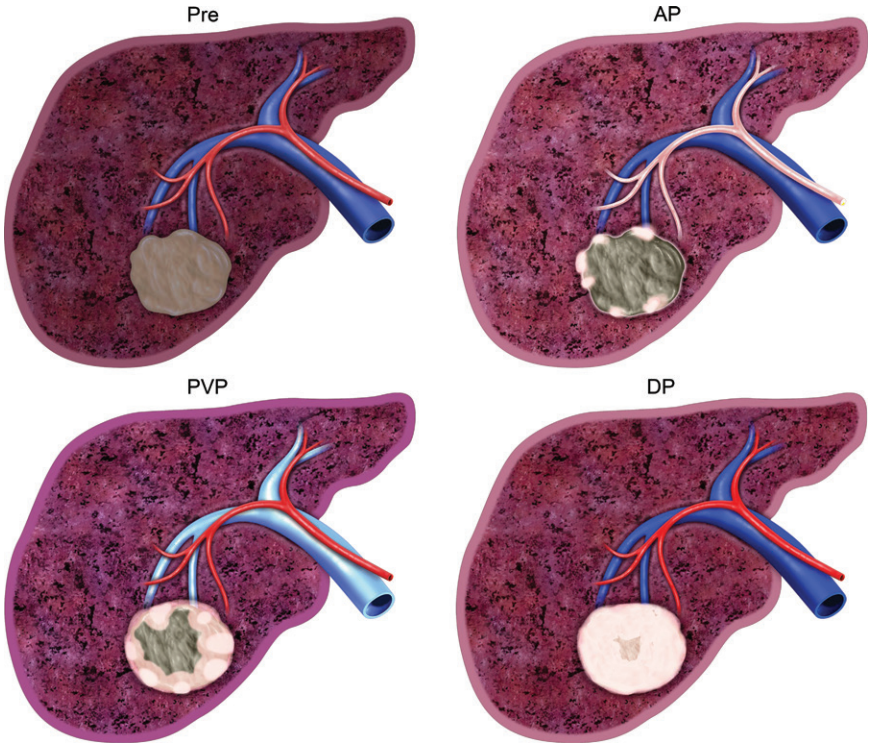

Figure 11. Peripheral discontinuous nodular enhancement is a classic description of the enhancement pattern associated with a hemangioma (pale brown lesion with no distinct features on precontrast *[pre]* images). It exhibits peripheral discontinuous nodular enhancement in the AP (peripheral puddles of bright pale pink that mirror the arteries), which progressively expands in the PVP (the peripheral puddles increase in size and become more and more continuous) owing to centripetal fill-in. Eventually, there is complete or near-complete contrast material filling of the lesion in the DP if the hemangioma is smaller, or sparing of a central scar in the case of a giant hemangioma.

fused by portal venules (53); therefore, they tend not to enhance in earlier phases. After the PVP, FC enhancement gradually increases as contrast material slowly accumulates in the collagen matrix when extracellular contrast agents are used. As US contrast material does not accumulate in the extracellular space, FCs are not apparent at CEUS (11,22).

Occasionally, delayed peripheral or periobservational enhancement may occur owing to compressed tissue, in the absence of a true FC. This phenomenon is referred to as a pseudocapsule. Since true FCs cannot be reliably distinguished from pseudocapsules at imaging (54), LI-RADS uses the term *enhancing capsule appearance* or *enhancing capsule* to include both of these entities (6,23). The enhancing capsule is a major feature of HCC in the CT and MRI diagnostic algorithm.

It is important to accurately distinguish an enhancing capsule from background fibrosis in a cirrhotic liver. Therefore, to qualify as a major feature of HCC in the CT and MRI LI-RADS (2), an enhancing capsule must be thicker or more conspicuous than fibrosis around background nodules (2,5,16,23,24). Furthermore, the enhancing capsule appearance associated with HCC must be smooth in contour and uniform in thickness and must surround all or most of the observation at CT or MRI (Fig 14). These latter features are useful in helping distinguish enhancing FCs from periobservational perfusion-related phenomena.

Capsule formation is associated with progressed HCCs exhibiting expansile growth (Fig 15) (55), and the capsule is associated with a better prognosis when intact (4,56). Among all HCCs, an enhancing capsule may be seen in approximately 40%–75% of cases, with the high variability partially attributable to the fact that the capsule may not be discernible if hepatobiliary agents are used (23,24,57). Some studies have shown that small HCCs (≤2 cm) can have an enhancing capsule with an even higher frequency, with rates as high as 93%–96% (23,57). Therefore, a capsule can be an important imaging feature even in smaller observations.

Capsule appearance should be differentiated from other peripheral and periobservational enhancement patterns (Fig 15). Rim APHE will peak in the early AP, corona enhancement will peak in the late AP and PVP, while enhancing capsule appearance occurs in the PVP or DP (6,25). The most commonly mistaken mimic of an enhancing capsule is a hyperintense rim in the HBP, which is caused by retention of contrast material in hyperplastic functional hepatocytes at the periphery of benign or malignant lesions (58). This finding is seen exclusively during the transitional phase and HBP, as opposed to an enhancing capsule, which is seen as early as the PVP.

Nonenhancing Capsule Appearance

Nonenhancing capsule appearance is defined as a hypointense rim on T1- and T2-weighted images

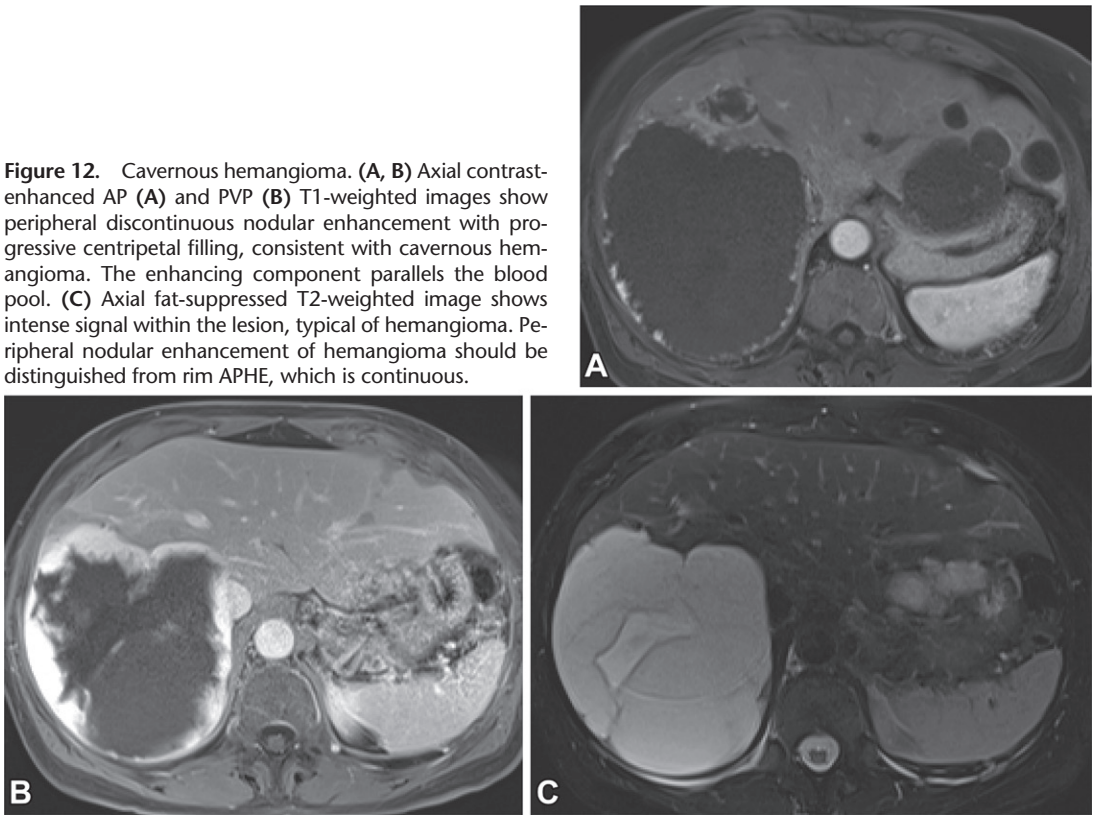

Figure 12. Cavernous hemangioma. **(A, B)** Axial contrast-enhanced AP **(A)** and PVP **(B)** T1-weighted images show peripheral discontinuous nodular enhancement with progressive centripetal filling, consistent with cavernous hemangioma. The enhancing component parallels the blood pool. **(C)** Axial fat-suppressed T2-weighted image shows intense signal within the lesion, typical of hemangioma. Peripheral nodular enhancement of hemangioma should be distinguished from rim APHE, which is continuous.

without appreciable enhancement in the postcontrast phases of CT and MRI (Fig 16) (4). It manifests as a hypointense rim in the HBP when hepatobiliary agents are used (4,24). The explanation of this finding is a fibrous capsule (FC) without appreciable enhancement at CT or MRI (3,24). The underlying pathophysiology remains unclear but may be due to decreased vascularity or smaller extracellular space in some FCs, such as in the setting of obstructed portal venous flow. This feature is considered an ancillary feature of HCC (2,16), although its effect on diagnostic accuracy in HCC is not well known (3).

A nonenhancing capsule should be thicker or more conspicuous than the fibrosis around the background regenerative nodules (3). Unlike peripheral washout, a nonenhancing capsule is smooth and discrete and shows persistent hypoenhancement in all postcontrast phases (Fig 17) (2).

Periobservational Features

Corona Enhancement

Corona enhancement is an ancillary feature favoring malignancy in general but not HCC in particular (16). It refers to periobservational enhancement as a result of early venous drainage of tumor into nearby hepatic sinusoids or portal venules (3,55,59). The draining venules can sometimes be seen as bright branching structures along the route of drainage of the central hepatic nodule (59). This periobservational enhancement is ringlike with variable thickness and flame-shaped borders, can be contiguous with part or all of an observation (3,5,26), and peaks during the late AP and early PVP, when the tumor starts to wash out (Fig 18) (3,27).

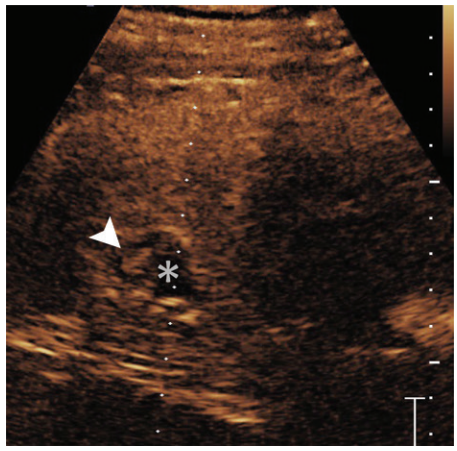

Figure 13. Peripheral nodular enhancement after microwave ablation in a 67-year-old man with nonalcoholic steatohepatitis (NASH)–related cirrhosis. CEUS image shows a hypoechoic observation in the posterior right lobe at the site of prior ablation (*) with peripheral nodular enhancement (arrowhead), concerning for residual viable disease (LI-RADS treatment response [LR-TR] viable). The ablation probe was reintroduced, and the area was re-treated.

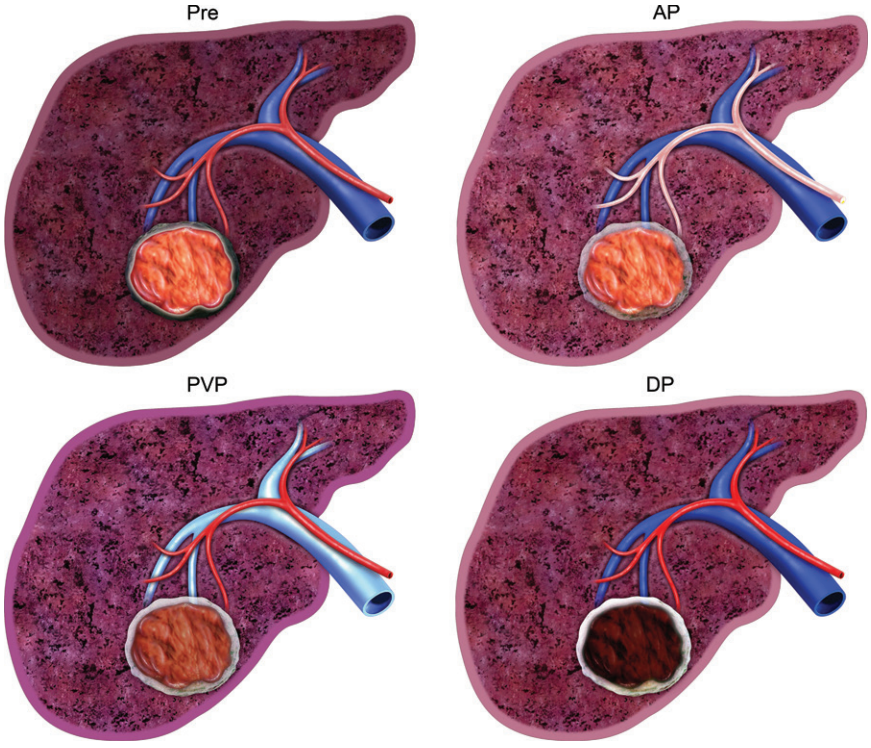

Figure 14. An enhancing capsule is neither directly intrinsic or extrinsic to the lesion, but is a stand-alone finding and not separable from the central lesion. On precontrast *(pre)* images, the central lesion may show a dark peripheral rim, which progressively enhances over time due to fibrous tissue in the capsule. (The dark rim on precontrast images becomes a brighter shade of gray in the AP and PVP, then becomes white in the DP.) Concurrently, the central lesion—especially in the case of HCC—may enhance in the AP and show central washout in the PVP and DP (the central orange-pink tissue is brightest in the AP and becomes darker in the PVP and DP).

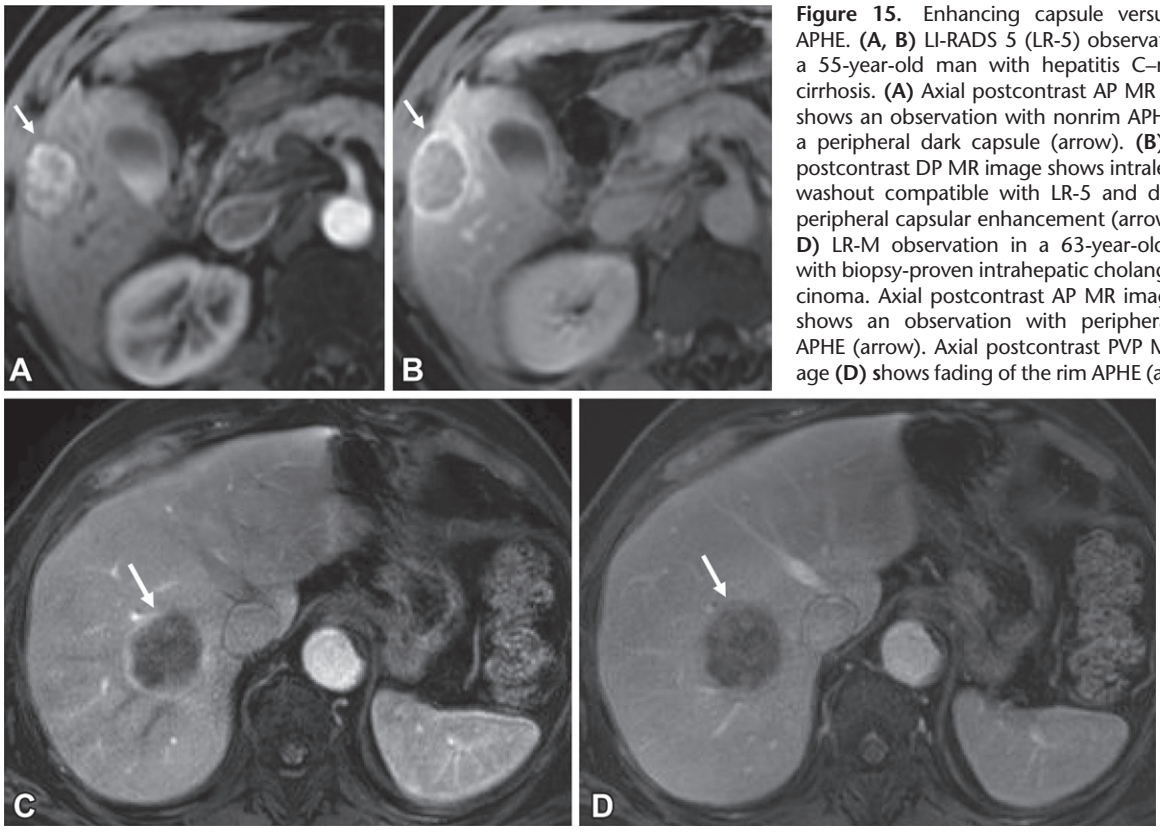

Figure 15. Enhancing capsule versus rim APHE. **(A, B)** LI-RADS 5 (LR-5) observation in a 55-year-old man with hepatitis C–related cirrhosis. **(A)** Axial postcontrast AP MR image shows an observation with nonrim APHE and a peripheral dark capsule (arrow). **(B)** Axial postcontrast DP MR image shows intralesional washout compatible with LR-5 and delayed peripheral capsular enhancement (arrow). **(C, D)** LR-M observation in a 63-year-old man with biopsy-proven intrahepatic cholangiocarcinoma. Axial postcontrast AP MR image **(C)** shows an observation with peripheral rim APHE (arrow). Axial postcontrast PVP MR image **(D)** shows fading of the rim APHE (arrow).

Since corona enhancement is partially due to increased vascularity in the surrounding tissue, it may be recognized at CEUS (11,22). According to some reports, corona enhancement is found in 60%–81% of HCCs at MRI (3,60,61). Early HCCs drain via hepatic veins rather than via sinusoids or portal venules; therefore, corona enhancement will not be seen in early-stage HCCs (55,62).

Corona enhancement may be confused with other patterns. Flame-shaped or lobulated

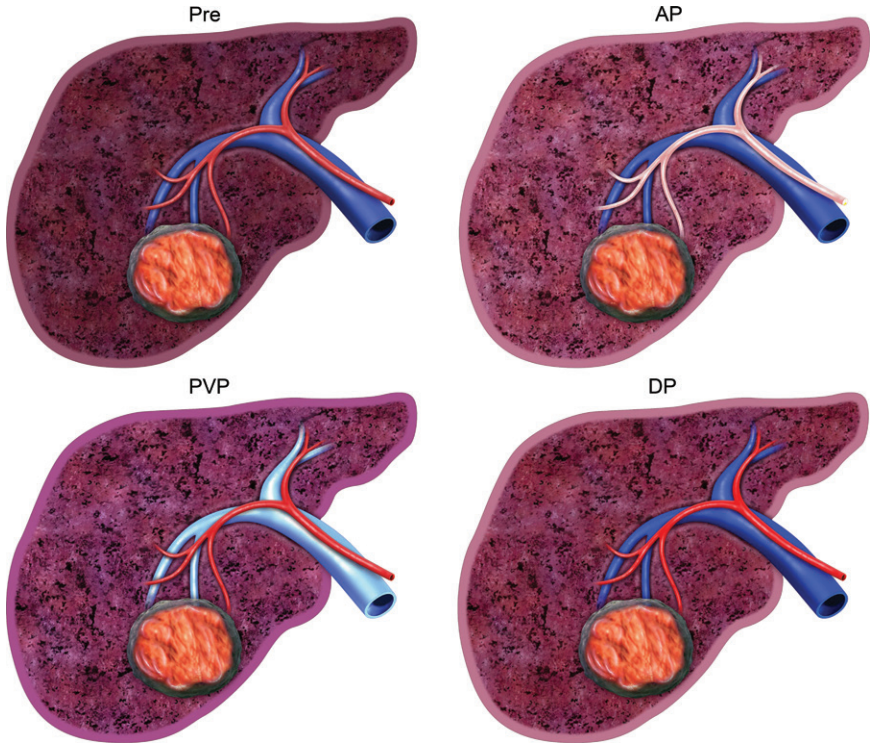

Figure 16. A nonenhancing capsule is neither directly intrinsic nor extrinsic to the observation, but is a stand-alone finding and not separable from the central aspect of the observation. It typically manifests as a dark peripheral rim on precontrast *(pre)* and postcontrast T1-weighted MR images.

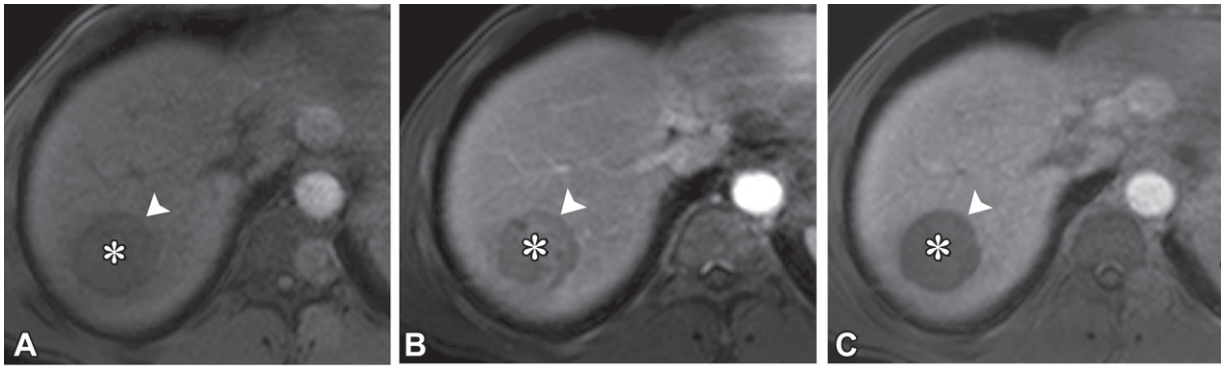

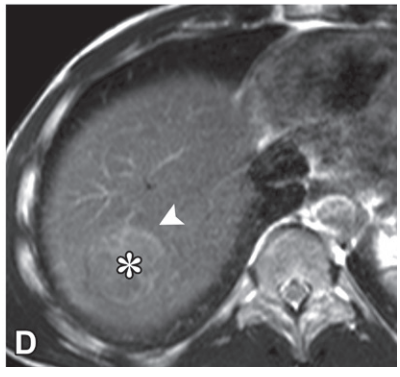

Figure 17. HCC in a 47-year-old man with chronic hepatitis B. Axial T1-weighted images show an observation (*) with a nonenhancing smooth rim (arrowhead) in all phases and with heterogeneous central enhancement in the AP **(B)**. The rim was compatible with a nonenhancing capsule.

morphology with variable thickness (Fig 19) helps distinguish corona enhancement from an enhancing capsule, which is a smooth discrete structure with uniform thickness (3). Corona enhancement and capsule appearance may coexist. HCC with an FC that contains intracapsular portal venules may show corona enhancement via portal venules in addition to an enhancing capsule appearance in later phases. The altered venous drainage is most appreciable during the AP and PVP and may not be apparent in more delayed postcontrast phases when equilibrium is reached (63,64).

There may possibly be an increased incidence of micrometastatic disease within the enhancing corona, when present (6). As such, the presence of corona enhancement is an important prognostic factor, and the region with corona enhancement should be considered in treatment planning, whether by surgery or ablation (3,6,65).

Arterioportal Shunting

Arterioportal shunts are commonly due to aberrant vasculature in the setting of cirrhosis, owing

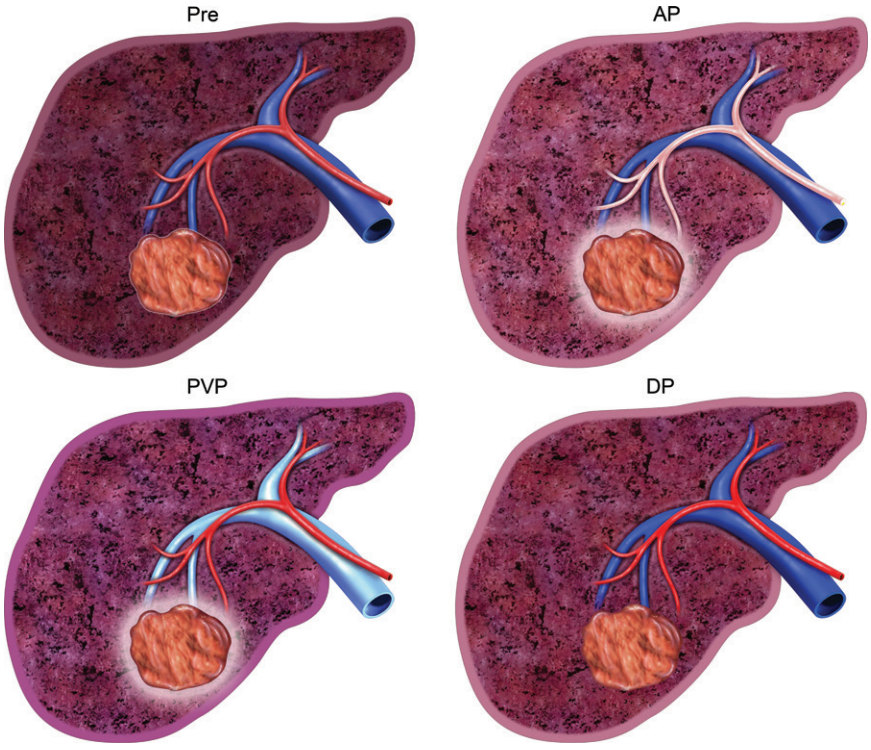

Figure 18. Corona enhancement appears as an irregular zone of surrounding enhancement in the late AP and PVP, depicted as an orange-pink lesion with a periobservational region of ill-defined bright enhancement in these phases. This enhancement localizes to the surrounding hepatic parenchyma rather than to the central lesion. It will not appear on precontrast *(pre)* images and is typically inconspicuous in the DP.

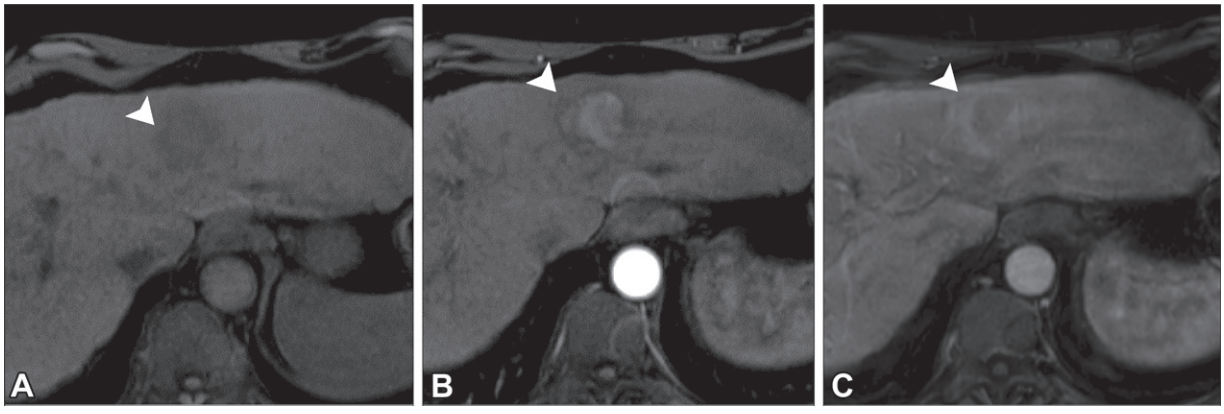

Figure 19. Corona enhancement associated with HCC in a 36-year-old woman with cirrhosis and underlying hepatitis C. **(A)** Axial precontrast T1-weighted image shows a hepatic observation (arrowhead) in the left hepatic lobe that is slightly hypointense to the surrounding liver. **(B)** On a corresponding postcontrast early AP image, the observation (arrowhead) has associated nonrim APHE with no corona enhancement. **(C)** Corresponding PVP image shows periobservational ill-defined enhancement of the adjacent background parenchyma (arrowhead), compatible with corona enhancement, along with intralesional washout.

to communication between a portal venule and hepatic arteriole with resultant alteration and redistribution of arterial flow. This communication can happen at different levels and in most instances is preexisting and physiologic. The existing connections between the arterioles and portal venules allow a compensatory increase in high-pressure arterial flow, via the hepatic arterial buffer response, whenever portal flow is decreased (66,67). Compromised portal flow can be the result of extrinsic compression, such as by a mass or thrombosis (18,28).

Arterioportal shunting classically manifests as wedge-shaped peripheral areas of transient hepatic intensity difference (THID) or transient hepatic attenuation difference (THAD) during the hepatic AP (Figs 20–22). This is best appreciated at multiphasic contrast-enhanced CT or MRI. Arterioportal shunts are not well seen at CEUS.

Focal shunts adjacent to a mass can occasionally mimic tumoral tissue (Fig 23). Attention to enhancement kinetics (such as lack of washout) and signal intensity with other sequences, when MRI is available, can help differentiate these entities (67). An arterioportal shunt associated with a mass may also mimic corona enhancement. These two phenomena can be distinguished, as

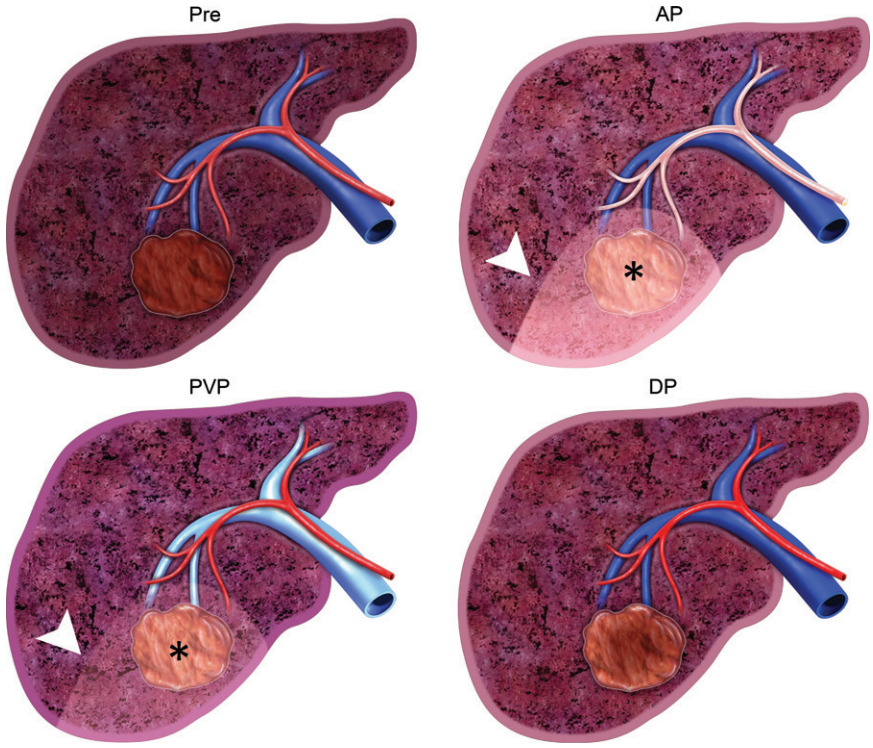

Figure 20. An arterioportal shunt is not seen on precontrast *(pre)* images, although a central obstructing mass may be seen (*). Characteristically, there is a wedge-shaped region of surrounding perilesional APHE (arrowhead) that can extend to the edge of the liver, due to the central obstructing mass. This enhancement fades in the early PVP and is no longer seen in the DP.

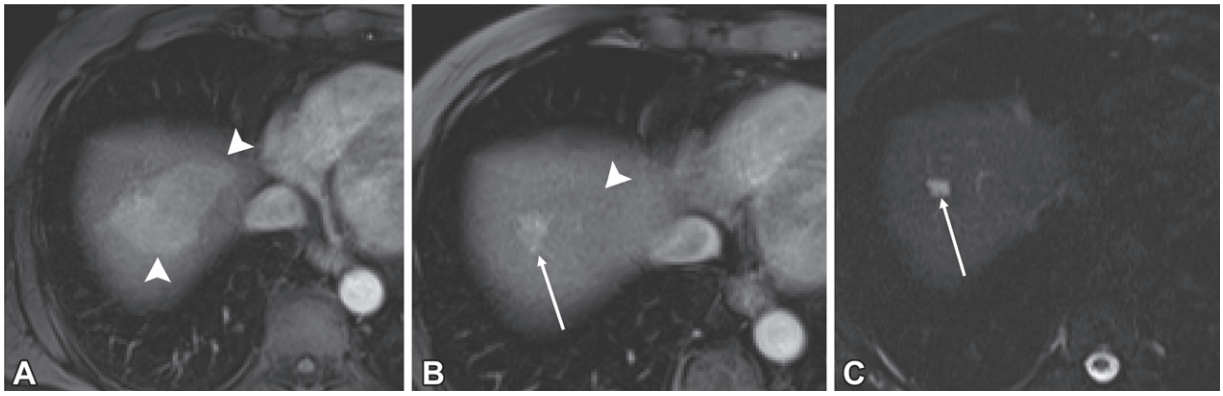

Figure 21. Periobservational arterioportal shunt. **(A)** Axial contrast-enhanced AP CT image shows a triangular area of enhancement (arrowheads) in the hepatic dome, consistent with an arterioportal shunt. **(B)** On a corresponding PVP image, the area of enhancement (arrowhead) has become isoenhancing to the background liver. The area of enhancement surrounds a flash-filling hemangioma (arrow). **(C)** Axial T2-weighted image shows typical hyperintensity of the hemangioma (arrow). Note that the area of the arterioportal shunt—which is better seen on the other images—is not associated with any signal intensity alteration.

a shunt will occur in the early AP, while corona enhancement will occur in the late AP and early PVP (16).

Local-Regional Therapy Response

Perilesional hyperemia is common after local-regional treatment of HCC and will typically resolve over time. Distinction between peripheral and perilesional imaging features after local-regional therapy has a profound effect on assignment of LI-RADS treatment response (LR-TR) viable, LR-TR equivocal, or LR-TR nonviable categories on the basis of the LI-RADS treatment response algorithm (Table 3) (16,72,73).

Nodular, masslike, or thick irregular tissue at or along the periphery of the treated lesion is concerning for viable tumor and is therefore categorized as LR-TR viable. Lack of any enhancement is compatible with LR-TR nonviable (Figs 24, 25) (68,69). When findings are uncertain and not definitively compatible with perilesional hyperemia or residual viable tumor, it would be appropriate to assign a response category of LR-TR equivocal (Fig 24).

Posttreatment imaging studies should be carefully compared with pretreatment imaging studies to assess the overlap of posttreatment enhancement with the location and margins of

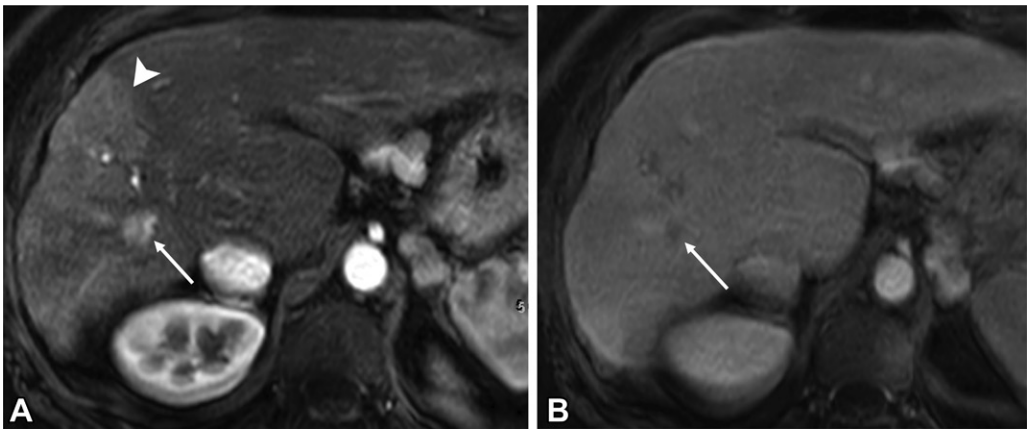

Figure 22. HCC in a 62-year-old man with hepatitis C–related cirrhosis. **(A)** Axial postcontrast AP MR image shows an observation with nonrim APHE (arrow) in the right hepatic lobe. The observation is located at the apex of a wedge-shaped area of enhancement (arrowhead). **(B)** On a corresponding DP MR image, the observation (arrow) shows internal washout characteristics, compatible with HCC. The wedge-shaped peripheral area of arterial enhancement has become isoenhancing to the background liver, compatible with arterioportal shunting.

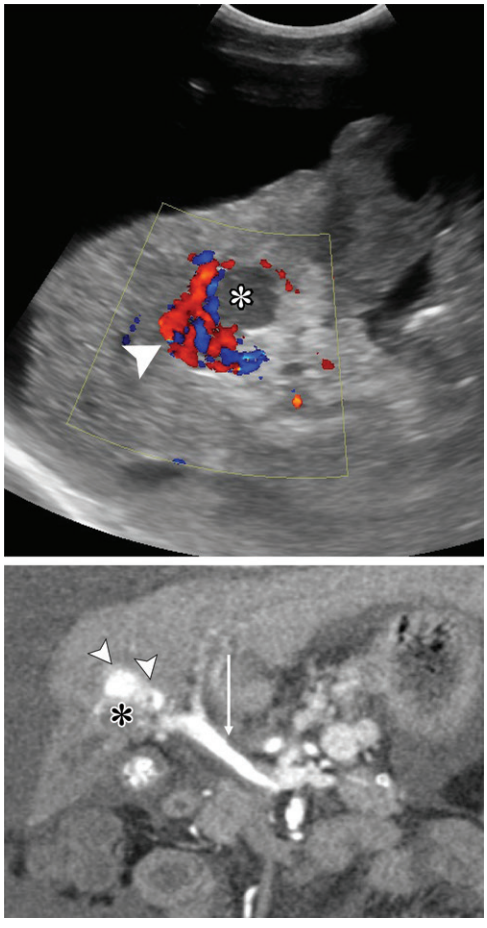

Figure 23. Arterioportal shunt mimicking a focus of HCC. Top: Duplex US image shows a hypoechoic lesion (*) with an adjacent nodular area of increased vascularity (arrowhead). Bottom: Coronal AP CT image shows hyperenhancing areas (arrowheads) superior to the mass (*) with early filling of the portal vein (arrow), suggestive of an arterioportal shunt between the feeding artery and draining vein of the tumor.

the original tumor, to better distinguish between expected posttreatment changes and residual tumor. Viable HCC after local-regional treatment may demonstrate a posttreatment necrotic core with peripheral hyperenhancing tissue (68,72). Therefore, LR-TR viable observations may exhibit imaging features mimicking rim APHE (Figs 24, 25), with peripheral irregular enhancement (Fig 13) similar to the pretreatment appearance, with nonperipheral washout (16).

Different local-regional treatments have different posttreatment imaging features that evolve over time. For example, after successful radiofrequency or microwave ablation, a tumor is expected to show no enhancement within the ablation zone (Figs 24, 25). Any other pattern of enhancement is considered to be compatible with the LR-TR equivocal or LR-TR viable category (Fig 25) (70,71).

On the other hand, a thin rim of peripheral enhancement is often seen immediately after cryoablation, which is attributed to benign reactive hyperemia. This enhancement can persist for up to several months. Thickened or irregular rim enhancement is worrisome for viable tumor.

In the case of percutaneous ethanol ablation and transarterial bland or chemoembolization, a thin peripheral enhancing rim due to granulation tissue can persist for months, categorized as LR-TR nonviable. When ill-defined geographic perilesional enhancement surrounds a treated lesion, it may be due to perfusion alteration; if not readily distinguishable from nodular enhancing viable tumor at the periphery of a treated lesion, it should be considered LR-TR equivocal.

Transarterial radioembolization (TARE) has a decreased embolic effect compared with that of other transcatheter therapies. Combined with the

Table 3: Peripheral and Periobservational Enhancement after Local-Regional Therapy

CT or MRI Finding	CEUS Finding	Type of Finding	Response to Local-Regional Therapy	LI-RADS Category
Enhancement surrounding treated lesion	Not applicable	Periobservational	Favorable	LR-TR nonviable
Enhancement surrounding and at periphery of treated lesion, often with a thin continuous rim	Enhancement surrounding and at periphery of treated lesion, often with a thin continuous rim	Peripheral or periobservational	Indeterminate	LR-TR equivocal
Enhancement at periphery of treated lesion, often with nodular foci	Enhancement at periphery of treated lesion, often with nodular foci	Peripheral	Unfavorable: concerning for residual or recurrent tumor	LR-TR viable

Source.—References 68–71.

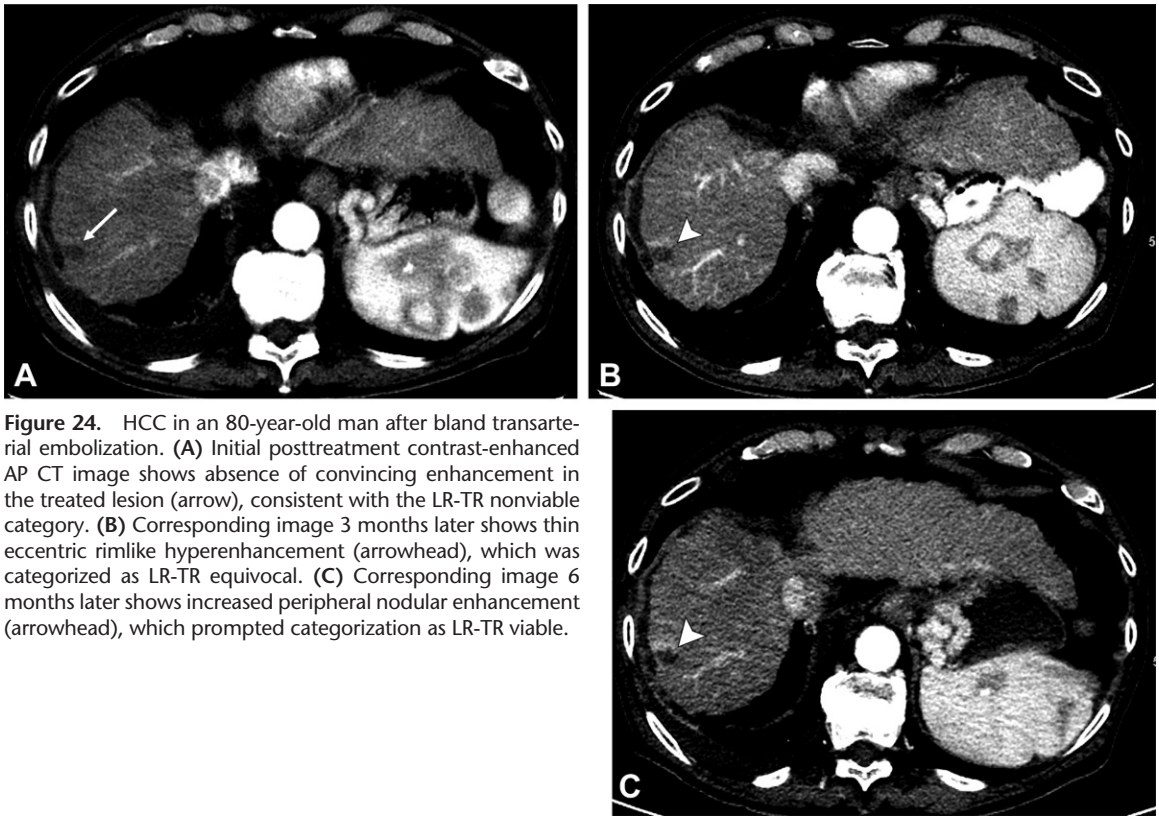

Figure 24. HCC in an 80-year-old man after bland transarterial embolization. **(A)** Initial posttreatment contrast-enhanced AP CT image shows absence of convincing enhancement in the treated lesion (arrow), consistent with the LR-TR nonviable category. **(B)** Corresponding image 3 months later shows thin eccentric rimlike hyperenhancement (arrowhead), which was categorized as LR-TR equivocal. **(C)** Corresponding image 6 months later shows increased peripheral nodular enhancement (arrowhead), which prompted categorization as LR-TR viable.

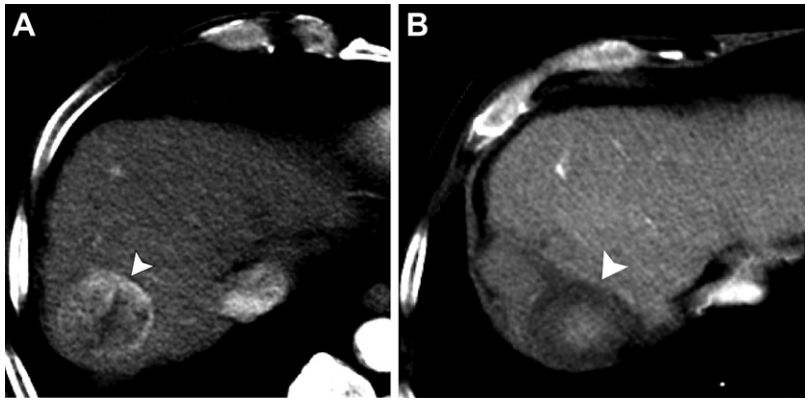

Figure 25. HCC in a 69-year-old man after yttrium 90 (^{90}Y) radioembolization. **(A)** Axial contrast-enhanced AP CT image shows enhancement in a previously treated lesion (arrowhead). This was categorized as an LR-TR viable observation. The patient was then treated with ^{90}Y radioembolization. **(B)** Corresponding image after ^{90}Y radioembolization no longer shows peripheral hyperenhancement in the lesion (arrowhead), consistent with LR-TR nonviable status. Note the postradioembolization changes surrounding the treated lesion in segment VII.

gradual effects of radiation, TARE can result in persistent tumoral enhancement in the first 3–6 months of follow-up imaging (70). Perilesional parenchymal hyperemia, often in a segmental distribution, also occurs during this early follow-up period, further challenging interpretation for residual viable tumor after TARE.

Conclusion

Peripheral and periobservational enhancement patterns can be grouped into various categories with different implications for the final LI-RADS score of the observation. Familiarity with these patterns and their contributing pathophysiology can improve assessment and characterization of liver observations. The peripheral and periobservational emerging features that are not defined or recognized by LI-RADS at this time are beyond the scope of this review, but they may also prove valuable in differential diagnosis of liver observations.

Acknowledgment.—We thank Kelly Kage for the illustrations.

Disclosures of Conflicts of Interest.—**C.B.S.** *Activities related to the present article:* disclosed no relevant relationships. *Activities not related to the present article:* grants from General Electric, Siemens, Philips, Bayer, Foundation for the National Institutes of Health, Gilead, and Pfizer; consultant for Blade, Boehringer, Epigenomics, AMRA, Bristol Myers Squibb, Exact Sciences, GE Digital, IBM-Watson, and Pfizer; laboratory service agreements with Enanta, Gilead, ICON, Intercept, NuSirt, Shire, Synageva, and Takeda; royalties from Wolters Kluwer; honoraria from Medscape; stock options in Livivos; advisory board for Quantix Bio. *Other activities:* disclosed no relevant relationships. **V.C.** *Activities related to the present article:* disclosed no relevant relationships. *Activities not related to the present article:* consultant for Bayer. *Other activities:* disclosed no relevant relationships. **D.T.F.** *Activities related to the present article:* disclosed no relevant relationships. *Activities not related to the present article:* research agreement with Philips Healthcare and Siemens Healthineers; equipment support from Philips Healthcare and Siemens Healthineers; payment for research activities from Philips Healthcare; research support (nonfinancial) from Bracco Diagnostics. *Other activities:* disclosed no relevant relationships. **K.J.F.** *Activities related to the present article:* disclosed no relevant relationships. *Activities not related to the present article:* consultant for GE, Bayer, and Median; grants from Pfizer, Bayer, GE, and Siemens. *Other activities:* disclosed no relevant relationships. **K.M.E.** *Activities related to the present article:* editorial board member of *RadioGraphics* (not involved in the handling of this article). *Activities not related to the present article:* disclosed no relevant relationships. *Other activities:* disclosed no relevant relationships.

References

1. Global Burden of Disease Cancer Collaboration; Fitzmaurice C, Akinyemiju TF, et al. Global, Regional, and National Cancer Incidence, Mortality, Years of Life Lost, Years Lived With Disability, and Disability-Adjusted Life-Years for 29 Cancer Groups, 1990 to 2016: A Systematic Analysis for the Global Burden of Disease Study. JAMA Oncol 2018;4(11):1553–1568.
2. American College of Radiology. Liver Reporting & Data System. https://www.acr.org/Clinical-Resources/Reporting-and-Data-Systems/LI-RADS. Accessed November 18, 2020.
3. Cerny M, Chernyak V, Olivié D, et al. LI-RADS version 2018 ancillary features at MRI. RadioGraphics 2018;38(7):1973–2001.
4. Elsayes KM, Hooker JC, Agrons MM, et al. 2017 version of LI-RADS for CT and MR imaging: an update. RadioGraphics 2017;37(7):1994–2017.
5. Chernyak V, Fowler KJ, Kamaya A, et al. Liver Imaging Reporting and Data System (LI-RADS) Version 2018: Imaging of Hepatocellular Carcinoma in At-Risk Patients. Radiology 2018;289(3):816–830.
6. Patella F, Pesapane F, Fumarola EM, et al. CT-MRI LI-RADS v2017: A Comprehensive Guide for Beginners. J Clin Transl Hepatol 2018;6(2):222–236.
7. Chernyak V, Santillan CS, Papadatos D, Sirlin CB. LI-RADS® algorithm: CT and MRI. Abdom Radiol (NY) 2018;43(1):111–126.
8. Wald C, Russo MW, Heimbach JK, Hussain HK, Pomfret EA, Bruix J. New OPTN/UNOS policy for liver transplant allocation: standardization of liver imaging, diagnosis, classification, and reporting of hepatocellular carcinoma. Radiology 2013;266(2):376–382.
9. Fowler KJ, Sheybani A, Parker RA 3rd, et al. Combined hepatocellular and cholangiocarcinoma (biphenotypic) tumors: imaging features and diagnostic accuracy of contrast-enhanced CT and MRI. AJR Am J Roentgenol 2013;201(2):332–339.
10. Mulé S, Galletto Pregliasco A, Tenenhaus A, et al. Multiphase Liver MRI for Identifying the Macrotrabecular-Massive Subtype of Hepatocellular Carcinoma. Radiology 2020;295(3):562–571.
11. Malone CD, Mattrey RF, Fetzer DT. Contrast-Enhanced Ultrasound (CEUS) for the Diagnosis and Management of Hepatocellular Carcinoma: Current Status and Future Trends. Curr Hepatol Rep 2016;15(4):307–316.
12. Baron RL, Peterson MS. From the RSNA refresher courses: screening the cirrhotic liver for hepatocellular carcinoma with CT and MR imaging—opportunities and pitfalls. RadioGraphics 2001;21(Spec No, suppl_1):S117–S132.
13. Barreiros AP, Piscaglia F, Dietrich CF. Contrast enhanced ultrasound for the diagnosis of hepatocellular carcinoma (HCC): comments on AASLD guidelines. J Hepatol 2012;57(4):930–932.
14. Niendorf E, Spilseth B, Wang X, Taylor A. Contrast Enhanced MRI in the Diagnosis of HCC. Diagnostics (Basel) 2015;5(3):383–398.
15. Rodgers SK, Fetzer DT, Gabriel H, et al. Role of US LI-RADS in the LI-RADS Algorithm. RadioGraphics 2019;39(3):690–708.
16. ACR LI-RADS Committee. CT/MRI LI-RADS v2018 CORE. https://www.acr.org/-/media/ACR/Files/RADS/LI-RADS/LI-RADS-2018-Core.pdf?la=en. Published 2018. Accessed December 24, 2020.
17. Kim YY, Kim MJ, Kim EH, Roh YH, An C. Hepatocellular Carcinoma versus Other Hepatic Malignancy in Cirrhosis: Performance of LI-RADS Version 2018. Radiology 2019;291(1):72–80.
18. Kim TK, Noh SY, Wilson SR, et al. Contrast-enhanced ultrasound (CEUS) Liver Imaging Reporting and Data System (LI-RADS) 2017: a review of important differences compared to the CT/MRI system. Clin Mol Hepatol 2017;23(4):280–289.
19. Loyer EM, Chin H, DuBrow RA, David CL, Eftekhari F, Charnsangavej C. Hepatocellular carcinoma and intrahepatic peripheral cholangiocarcinoma: enhancement patterns with quadruple phase helical CT—a comparative study. Radiology 1999;212(3):866–875.
20. Kim YY, Choi JY, Kim SU, et al. MRI Ancillary Features for LI-RADS Category 3 and 4 Observations: Improved Categorization to Indicate the Risk of Hepatic Malignancy. AJR Am J Roentgenol 2020;215(6):1354–1362.
21. Semelka RC, Brown ED, Ascher SM, et al. Hepatic hemangiomas: a multi-institutional study of appearance on T2-weighted and serial gadolinium-enhanced gradient-echo MR images. Radiology 1994;192(2):401–406.
22. D'Onofrio M, Crosara S, De Robertis R, Canestrini S, Mucelli RP. Contrast-Enhanced Ultrasound of Focal Liver Lesions. AJR Am J Roentgenol 2015;205(1):W56–W66.
23. Dioguardi Burgio M, Picone D, Cabibbo G, Midiri M, Lagalla R, Brancatelli G. MR imaging features of hepatocellular carcinoma capsule appearance in cirrhotic liver: comparison of

gadoxetic acid and gadobenate dimeglumine. Abdom Radiol (NY) 2016;41(8):1546–1554.
24. Kim B, Lee JH, Kim JK, Kim HJ, Kim YB, Lee D. The capsule appearance of hepatocellular carcinoma in gadoxetic acid-enhanced MR imaging: correlation with pathology and dynamic CT. Medicine (Baltimore) 2018;97(25):e11142.
25. Granata V, Fusco R, Avallone A, et al. Major and ancillary magnetic resonance features of LI-RADS to assess HCC: an overview and update. Infect Agent Cancer 2017;12(1):23.
26. Ahn SY, Lee JM, Joo I, et al. Prediction of microvascular invasion of hepatocellular carcinoma using gadoxetic acid-enhanced MR and (18)F-FDG PET/CT. Abdom Imaging 2015;40(4):843–851.
27. Motosugi U, Ichikawa T, Sou H, et al. Distinguishing hypervascular pseudolesions of the liver from hypervascular hepatocellular carcinomas with gadoxetic acid–enhanced MR imaging. Radiology 2010;256(1):151–158.
28. Kim TK, Choi BI, Han JK, Chung JW, Park JH, Han MC. Nontumorous arterioportal shunt mimicking hypervascular tumor in cirrhotic liver: two-phase spiral CT findings. Radiology 1998;208(3):597–603.
29. Kambadakone AR, Fung A, Gupta RT, et al. LI-RADS technical requirements for CT, MRI, and contrast-enhanced ultrasound. Abdom Radiol (NY) 2018;43(1):56–74. [Published correction appears in Abdom Radiol (NY) 2018;43(1):240.]
30. Grazioli L, Morana G, Caudana R, et al. Hepatocellular carcinoma: correlation between gadobenate dimeglumine-enhanced MRI and pathologic findings. Invest Radiol 2000;35(1):25–34.
31. McEvoy SH, Lavelle LP, Malone DE. Optimal timing of the delayed phase in dynamic contrast-enhanced imaging of the liver. Radiology 2013;269(2):619.
32. Cortis K, Liotta R, Miraglia R, Caruso S, Tuzzolino F, Luca A. Incorporating the hepatobiliary phase of gadobenate dimeglumine-enhanced MRI in the diagnosis of hepatocellular carcinoma: increasing the sensitivity without compromising specificity. Acta Radiol 2016;57(8):923–931.
33. Kirchin MA, Pirovano GP, Spinazzi A. Gadobenate dimeglumine (Gd-BOPTA): an overview. Invest Radiol 1998;33(11):798–809.
34. Pang EHT, Chan A, Ho SG, Harris AC. Contrast-Enhanced Ultrasound of the Liver: Optimizing Technique and Clinical Applications. AJR Am J Roentgenol 2018;210(2):320–332.
35. Lindner JR. Microbubbles in medical imaging: current applications and future directions. Nat Rev Drug Discov 2004;3(6):527–532.
36. Frydrychowicz A, Lubner MG, Brown JJ, et al. Hepatobiliary MR imaging with gadolinium-based contrast agents. J Magn Reson Imaging 2012;35(3):492–511.
37. Hope TA, Fowler KJ, Sirlin CB, et al. Hepatobiliary agents and their role in LI-RADS. Abdom Imaging 2015;40(3):613–625.
38. Kawata S, Murakami T, Kim T, et al. Multidetector CT: diagnostic impact of slice thickness on detection of hypervascular hepatocellular carcinoma. AJR Am J Roentgenol 2002;179(1):61–66.
39. Marin D, Catalano C, De Filippis G, et al. Detection of hepatocellular carcinoma in patients with cirrhosis: added value of coronal reformations from isotropic voxels with 64-MDCT. AJR Am J Roentgenol 2009;192(1):180–187.
40. Ichikawa T, Okada M, Kondo H, et al. Recommended iodine dose for multiphasic contrast-enhanced mutidetector-row computed tomography imaging of liver for assessing hypervascular hepatocellular carcinoma: multicenter prospective study in 77 general hospitals in Japan. Acad Radiol 2013;20(9):1130–1136.
41. Semelka RC, Helmberger TKG. Contrast agents for MR imaging of the liver. Radiology 2001;218(1):27–38.
42. Lee HS, Kim MJ, An C. How to utilize LR-M features of the LI-RADS to improve the diagnosis of combined hepatocellular-cholangiocarcinoma on gadoxetate-enhanced MRI? Eur Radiol 2019;29(5):2408–2416.
43. Fowler KJ, Potretzke TA, Hope TA, Costa EA, Wilson SR. LI-RADS M (LR-M): definite or probable malignancy, not specific for hepatocellular carcinoma. Abdom Radiol (NY) 2018;43(1):149–157.
44. Kim YY, Choi JY, Sirlin CB, An C, Kim MJ. Pitfalls and problems to be solved in the diagnostic CT/MRI Liver Imaging Reporting and Data System (LI-RADS). Eur Radiol 2019;29(3):1124–1132.
45. Balci NC, Semelka RC, Noone TC, et al. Pyogenic hepatic abscesses: MRI findings on T1- and T2-weighted and serial gadolinium-enhanced gradient-echo images. J Magn Reson Imaging 1999;9(2):285–290.
46. Popescu A, Sporea I, Sirli R, et al. Does contrast enhanced ultrasound improve the management of liver abscesses? A single centre experience. Med Ultrason 2015;17(4):451–455.
47. Kim SH, Lim HK, Lee WJ, Choi D, Park CK. Scirrhous hepatocellular carcinoma: comparison with usual hepatocellular carcinoma based on CT-pathologic features and long-term results after curative resection. Eur J Radiol 2009;69(1):123–130.
48. Huang M, Liao B, Xu P, et al. Prediction of Microvascular Invasion in Hepatocellular Carcinoma: Preoperative Gd-EOB-DTPA Dynamic Enhanced MRI and Histopathological Correlation. Contrast Media Mol Imaging 2018;2018:9674565.
49. Hu H, Zheng Q, Huang Y, et al. A non-smooth tumor margin on preoperative imaging assesses microvascular invasion of hepatocellular carcinoma: a systematic review and meta-analysis. Sci Rep 2017;7(1):15375.
50. Wang WT, Yang L, Yang ZX, et al. Assessment of Microvascular Invasion of Hepatocellular Carcinoma with Diffusion Kurtosis Imaging. Radiology 2018;286(2):571–580.
51. Brancatelli G, Federle MP, Blachar A, Grazioli L. Hemangioma in the cirrhotic liver: diagnosis and natural history. Radiology 2001;219(1):69–74.
52. International Consensus Group for Hepatocellular Neoplasia. Pathologic diagnosis of early hepatocellular carcinoma: a report of the International Consensus Group for Hepatocellular Neoplasia. Hepatology 2009;49(2):658–664.
53. Ohashi M, Wakai T, Korita PV, Ajioka Y, Shirai Y, Hatakeyama K. Histological evaluation of intracapsular venous invasion for discrimination between portal and hepatic venous invasion in hepatocellular carcinoma. J Gastroenterol Hepatol 2010;25(1):143–149.
54. Kim KA, Kim MJ, Jeon HM, et al. Prediction of microvascular invasion of hepatocellular carcinoma: usefulness of peritumoral hypointensity seen on gadoxetate disodium–enhanced hepatobiliary phase images. J Magn Reson Imaging 2012;35(3):629–634.
55. Choi JY, Lee JM, Sirlin CB. CT and MR imaging diagnosis and staging of hepatocellular carcinoma. I. Development, growth, and spread: key pathologic and imaging aspects. Radiology 2014;272(3):635–654.
56. Ng IOL, Lai ECS, Ng MM, Fan ST. Tumor encapsulation in hepatocellular carcinoma: a pathologic study of 189 cases. Cancer 1992;70(1):45–49.
57. Rimola J, Forner A, Tremosini S, et al. Non-invasive diagnosis of hepatocellular carcinoma ≤2 cm in cirrhosis: diagnostic accuracy assessing fat, capsule and signal intensity at dynamic MRI. J Hepatol 2012;56(6):1317–1323.
58. Fujita N, Nishie A, Asayama Y, et al. Hyperintense Liver Masses at Hepatobiliary Phase Gadoxetic Acid–enhanced MRI: Imaging Appearances and Clinical Importance. RadioGraphics 2020;40(1):72–94.
59. Kitao A, Zen Y, Matsui O, Gabata T, Nakanuma Y. Hepatocarcinogenesis: multistep changes of drainage vessels at CT during arterial portography and hepatic arteriography—radiologic-pathologic correlation. Radiology 2009;252(2):605–614.
60. Ronot M, Fouque O, Esvan M, Lebigot J, Aubé C, Vilgrain V. Comparison of the accuracy of AASLD and LI-RADS criteria for the non-invasive diagnosis of HCC smaller than 3 cm. J Hepatol 2018;68(4):715–723.
61. Kim H, Park MS, Choi JY, et al. Can microvessel invasion of hepatocellular carcinoma be predicted by pre-operative MRI? Eur Radiol 2009;19(7):1744–1751.
62. Yoshida K, Kobayashi S, Matsui O, et al. Hepatic pseudolymphoma: imaging-pathologic correlation with special reference to hemodynamic analysis. Abdom Imaging 2013;38(6):1277–1285.

63. Ueda K, Matsui O, Kawamori Y, et al. Hypervascular hepatocellular carcinoma: evaluation of hemodynamics with dynamic CT during hepatic arteriography. Radiology 1998;206(1):161–166.
64. Miyayama S, Yamashiro M, Okuda M, et al. Detection of corona enhancement of hypervascular hepatocellular carcinoma by C-arm dual-phase cone-beam CT during hepatic arteriography. Cardiovasc Intervent Radiol 2011;34(1):81–86.
65. Sakon M, Nagano H, Nakamori S, et al. Intrahepatic recurrences of hepatocellular carcinoma after hepatectomy: analysis based on tumor hemodynamics. Arch Surg 2002;137(1):94–99.
66. Elsayes KM, Shaaban AM, Rothan SM, et al. A comprehensive approach to hepatic vascular disease. RadioGraphics 2017;37(3):813–836.
67. Kim KW, Kim AY, Kim TK, et al. Hepatic hemangiomas with arterioportal shunt: sonographic appearances with CT and MRI correlation. AJR Am J Roentgenol 2006;187(4):W406–W414.
68. Do RK, Mendiratta-Lala M. LI-RADS Version 2018 Treatment Response Algorithm: The Evidence Is Accumulating. Radiology 2020;294(2):327–328.
69. Chaudhry M, McGinty KA, Mervak B, et al. The LI-RADS Version 2018 MRI Treatment Response Algorithm: Evaluation of Ablated Hepatocellular Carcinoma. Radiology 2020;294(2):320–326.
70. Voizard N, Cerny M, Assad A, et al. Assessment of hepatocellular carcinoma treatment response with LI-RADS: a pictorial review. Insights Imaging 2019;10(1):121.
71. Guan YS, Sun L, Zhou XP, Li X, Zheng XH. Hepatocellular carcinoma treated with interventional procedures: CT and MRI follow-up. World J Gastroenterol 2004;10(24):3543–3548.
72. Gervais DA. LI-RADS treatment response algorithm: performance and diagnostic accuracy. Radiology 2019;292(1):235–236.
73. Shropshire EL, Chaudhry M, Miller CM, et al. LI-RADS Treatment Response Algorithm: Performance and Diagnostic Accuracy. Radiology 2019;292(1):226–234.